Acta Materialia 138 (2017) 52–60

Contents lists available at ScienceDirect

Acta Materialia

journal homepage: www.elsevier.com/locate/actamat

Full length article

Indentation size effect in nanoporous gold

Young-Cheon Kim [a, 1, 2], Eun-Ji Gwak [a, 2], Seung-min Ahn [a], Jae-il Jang [b], Heung Nam Han [c], Ju-Young Kim [a, d, *]

[a] School of Materials Science and Engineering, UNIST (Ulsan National Institute of Science and Technology), Ulsan 44919, Republic of Korea
[b] Division of Materials Science and Engineering, Hanyang University, Seoul 04763, Republic of Korea
[c] School of Materials Science and Engineering, Seoul National University, Seoul 08826, Republic of Korea
[d] KIST-UNIST Ulsan Center for Convergent Materials, UNIST, Ulsan 44919, Republic of Korea

ARTICLE INFO

Article history:
Received 24 February 2017
Received in revised form
14 July 2017
Accepted 17 July 2017
Available online 24 July 2017

Keywords:
Nanoporous gold
Nanoindentation
Porous materials
Hardness
Indentation size effect

ABSTRACT

We find that hardness of nanoporous gold (np-Au) measured by nanoindentation tends to increase with decreasing indentation depth, similar to the indentation size effect (ISE) in solid materials. While ISE in solid materials is attributed to a local increase in density of geometrically necessary dislocations (GNDs), the origin of ISE in np-Au has not been studied systematically. We prepare four np-Au samples with ligament sizes of 26, 73, 126, and 630 nm by free corrosion dealloying and post heat treatments. For the normalized hardness (hardness/macroscopic hardness) vs normalized indentation depth (indentation depth/three times ligament size), we find that the ISE trends for three np-Au samples of ligament sizes 26, 73, and 127 nm are almost identical, while an enhanced ISE is shown for np-Au with greatest ligament size, 630 nm. We investigate ISE in np-Au based on nanomechanics model for nanoindentation on np-Au with a sharp indenter, uniaxial compression and pure shear testing for np-Au.

1. Introduction

Nanoporous gold (np-Au) has received significant attention for such possible applications as sensors, actuators, and catalysis due to its high specific surface area and chemical stability [1–14]. Studies on the mechanical properties of np-Au have been numerous because its fragility is critical in applications [15,16]. Previous research revealed that the strength of np-Au depends strongly on ligament size as well as relative density. Li and Sieradzki [17] suggested a ductile-brittle transition in three-point bending based on change in slope of the relation between fracture strain/stress and ligament size. Biener et al. [18] found that nanoindentation hardness depends on ligament size; hardness increases with decreasing ligament size. Using the Gibson-Ashby model on foam plasticity, they suggested that the ligament yield strength approaches the theoretical strength of Au that the yield strength of np-Au, evaluated from nanoindentation hardness, can be as strong as solid Au in spite of its porous structure. Volkert et al. [19] showed that the compressive strength of np-Au micro-pillars depends on ligament size rather than micro-pillar diameter, and that the strength of individual ligaments attains the theoretical strength of Au. They confirmed a distinction between elastic and plastic behavior of solid materials depending on sample size (diameter of single-crystalline nanopillars and ligament size in np-Au). They explained the trend in mechanical behavior of Au samples with external size ranging from 10 to 10^5 nm by the Gibson-Ashby model [20] estimated for np-Au, nanobox Au, and single-crystalline Au nanopillars. Yield strength is strongly dependent on external sample size below 50 μm, while elastic modulus is independent of sample size. Hodge et al. [21] showed that the mechanical behavior of np-Au is strongly dependent on ligament size, in contrast with previous studies finding that cell size, including ligaments and pores, had a minimal effect on mechanical properties in macrocellular materials of similar relative density. They suggested a modified scaling equation for the yield strength of np-Au as a function of ligament size and relative density by incorporating a Hall-Petch-type relation coefficient. They noted that np-Au follows the Gibson-Ashby model as ligament size approaches 1 μm from sub-micron size. From numerous experimental results, Briot and Balk [22] suggested a universal scaling law for yield strength of np-

* Corresponding author. School of Materials Science and Engineering, UNIST (Ulsan National Institute of Science and Technology), Ulsan 44919, Republic of Korea.
E-mail address: juyoung@unist.ac.kr (J.-Y. Kim).
[1] Present address: System Convergence Technology Division, Mechanical Safety Technology Center, Korea Testing Laboratory, Jinju-si 52852, Republic of Korea.
[2] These authors contributed to this work equally.

http://dx.doi.org/10.1016/j.actamat.2017.07.040
1359-6454/

Au in which ligament size effect is significant only for ligament size smaller than 1 μm. Saane et al. [23] studied mechanical properties of np-Au using atomistic and continuum simulations; they found that elastic modulus depends strongly on relative density and crystallographic orientation, and yield strength depends on relative density. They found that the exponent in a scaling law determined from simulation results is higher than that using the Gibson-Ashby model, and explained this result by the loss of connectivity in np-Au.

The trend of nanoindentation hardness vs indentation depth for np-Au in previous studies is that hardness tends to increase with decreasing indentation depth, which is similar to indentation size effect (ISE) in solid materials. The ISE in solids is explained by saying that the density of geometrically necessary dislocations (GNDs) increases as indentation depth decrease, while density of statistically stored dislocations (SSDs) is independent of indentation depth [24–30]. The ISE in np-Au cannot, of course, be explained by this classical ISE mechanism. GNDs generated in ligaments of np-Au could easily escape at the free surface due to the typically sub-micron scale of ligament, and ligaments could collapse easily into the extensive neighboring free volume (pores), rather than undergoing plastic constraint as in solid materials. ISE in np-Au has not been studied systemically but could be critical, especially when indentation depth is limited to within the shallow indentation depth where ISE is pronounced.

Here we investigate ligament-size-dependent ISE in np-Au. To separate ISE elements coming from porous structure and ligament-size dependency, we used np-Au samples of four ligament sizes, 26, 73, 127, and 630 nm, to obtain the relation between normalized hardness – the ratio of hardness to macroscopic hardness (i.e., hardness at sufficient indentation depth – and normalized indentation depth (i.e., the ratio of indentation depth to length scale of one unit cell composed of one ligament and one pore assumed to be three times ligament size)). We find a clear transition in ISE in normalized hardness vs normalized indentation depth for our four np-Au samples: the trends in the ISE for the three np-Au samples of small ligament size (26, 73, 127 nm) are almost identical, but the ISE for np-Au with greatest ligament size (630 nm) is enhanced over the other three. To explain this result, we suggest a novel ISE model for np-Au in which during nanoindentation, initial plastic collapse of np-Au occurs at the contact boundary between nanoindenter and np-Au primarily by shear force, and the collapsed np-Au placed beneath nanoindenter expands primarily by compressive force. Using uniaxial compression and pure shear tests, we discuss the origin of ligament-size-dependent ISE in np-Au.

2. Experiments

Four np-Au samples of ligament sizes 26 (±4.0), 73 (±8.8), 127 (±12.8), 630 (±61.4) nm were prepared as shown in Fig. 1(a)–(d). To prepare the precursor alloy of Au 30 at.% and Ag 70 at.%, Au (99.99%) and Ag (99.99%) pellets were melted together by plasma arc-melting in an Ar environment, held at 800 °C for 72 h in a tube furnace under N_2 environment for homogenization, and slowly cooled to room temperature in the furnace. The spherical samples were compressed into round disks using universal mechanical tester (Instron 5982). Both sides of the alloys were gently mechanically polished down to 0.25 μm diamond suspension. The precursor alloys were round discs of diameter ~8 mm and thickness ~1 mm. The samples were annealed in a tube furnace under N_2 environment at 800 °C for 24 h to homogenize them further and to release any residual stress induced during mechanical compression and polishing.

The np-Au samples were prepared from the precursor $Au_{30}Ag_{70}$ alloys by free-corrosion dealloying. To control ligament size, dealloying was carried out in nitric acid solutions under different conditions: in mixture of 2:1 70% concentrated nitric acid to DI water at 20 °C for 72 h, resulting in ligament size (l) 26 nm (hereafter called sample #1 ($l = 26$ nm)), in mixture of 1:1 of 70% concentrated nitric acid to DI water at 50 °C for 72 h, resulting in ligament size 73 nm (hereafter called sample #2 ($l = 73$ nm)), and in mixture of 1:1 of 70% concentrated nitric acid to DI water at 80 °C for 72 h, resulting in ligament size 127 nm (hereafter called sample #3 ($l = 127$ nm)). These dealloying conditions were based on the authors' previous work [31]. Through additional heat treatment of sample #3 ($l = 127$ nm) at 600 °C for 2 h, np-Au samples of ligament size 630 nm were obtained (hereafter called sample #4 ($l = 630$ nm)). The np-Au samples were examined in field emission scanning electron microscopy (FE-SEM, FEI Nanonova 230). Ligament sizes were evaluated by thickness of necks at the ligament center, their thinnest part, from at least 100 measurements in SEM images. Since homogeneity in ligament size distribution could affect ISE in np-Au, we measured ligament sizes for cross sections prepared by focused ion beam (FIB, Quanta 3D FEG) milling as shown in Fig. 1(e)~(h). Fig. 1(i) shows that ligament size normalized by average ligament size measured for top SEM images is almost one throughout the nanoindentation loading direction from the free surface, which indicates that the size of ligaments corresponding to volume from free surface to maximum indentation depth is uniform for samples #1~#4.

Nanoindentations using three-sided Berkovich indenter were performed on samples #1 through #4. For each sample, at least 12 reproducible nanoindentation force-depth curves were obtained. Maximum indentation depths for each sample were determined as 40 times of their ligament size, where cell size D is composed of one ligament and one neighboring pore, assumed here to be three times ligament size, $3l$ as shown in Fig. 6(f); that is, intended maximum indentation depth = $13.3D = 40l$. Indented volume by this maximum indentation depth approximately contains 27000 cells, and we confirmed that convergent trend in hardness with increasing indentation depth is well-described up to this maximum indentation depth. Continuous stiffness measurement (CSM) nanoindentations were carried out by XP and DCM II modules with maximum load capacity 500 and 30 mN in a G200 nanoindenter (Keysight Co.), respectively. All nanoindentation tests were conducted at constant indentation strain rate 0.05 s^{-1}, with allowable thermal drift limit of 0.05 nm/s. Relative densities of the samples were evaluated from measurements of external volume and sample weight. Np-Au cuboids of dimensions 0.8 mm × 0.8 mm × 1.2 mm for testing in both uniaxial compression and pure shear were prepared. Compression and shear tests were performed at constant displacement rate of 0.05 s^{-1} using a micro universal testing machine (Instron 5948). For each sample, at least 4 reproducible force-displacement curves were obtained for compression and shear tests.

3. Results and discussion

3.1. ISE in np-Au

Fig. 2 shows typical indentation force-depth curves and hardness as a function of indentation depth for four np-Au samples. Fig. 2(a)–(d) show that greater force is required to attain same indentation depth as ligament size decreases, which is in line with the higher hardness found for smaller ligament size in previous researches [21]. Fig. 2(e)–(h) show an increase in hardness with decreasing indentation depth for all np-Au samples, i.e. an ISE in np-Au. A convergent hardness value as indentation depth increases is measured by averaging hardness values between indentation depths $30l$ and $40l$, the maximum indentation depth. This

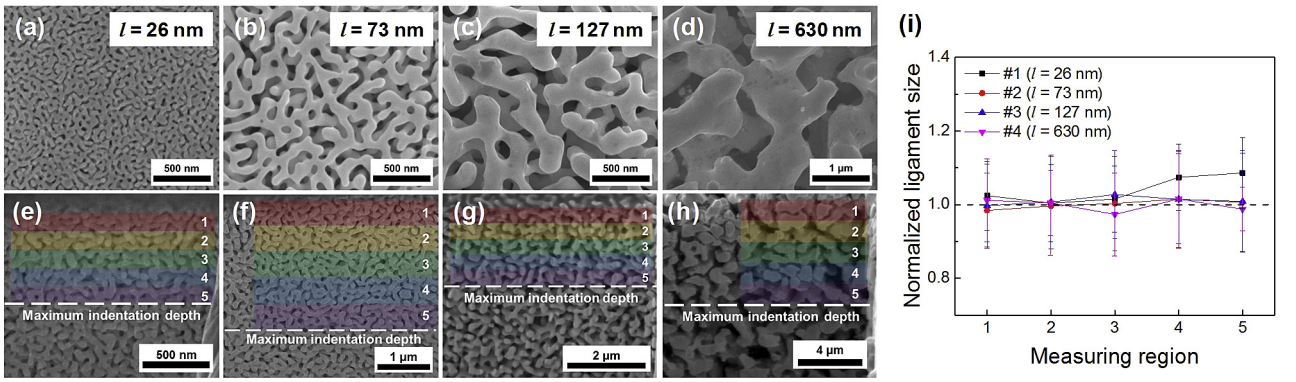

Fig. 1. SEM images (a)~(d) at top view and (e)~(h) cross-sections prepared by FIB milling. Colored regions 1 through 5 indicate a fifth of the maximum indentation depth from top surface. (a), (e) sample #1 (l = 26 nm), (b), (f) sample #2 (l = 73 nm), (c), (g) sample #3 (l = 126 nm), and (d), (h) sample #4 (l = 630 nm). (i) Ligament size normalized by average ligament size measured for top surface as a function of depth from free surface. (For interpretation of the references to colour in this figure legend, the reader is referred to the web version of this article.)

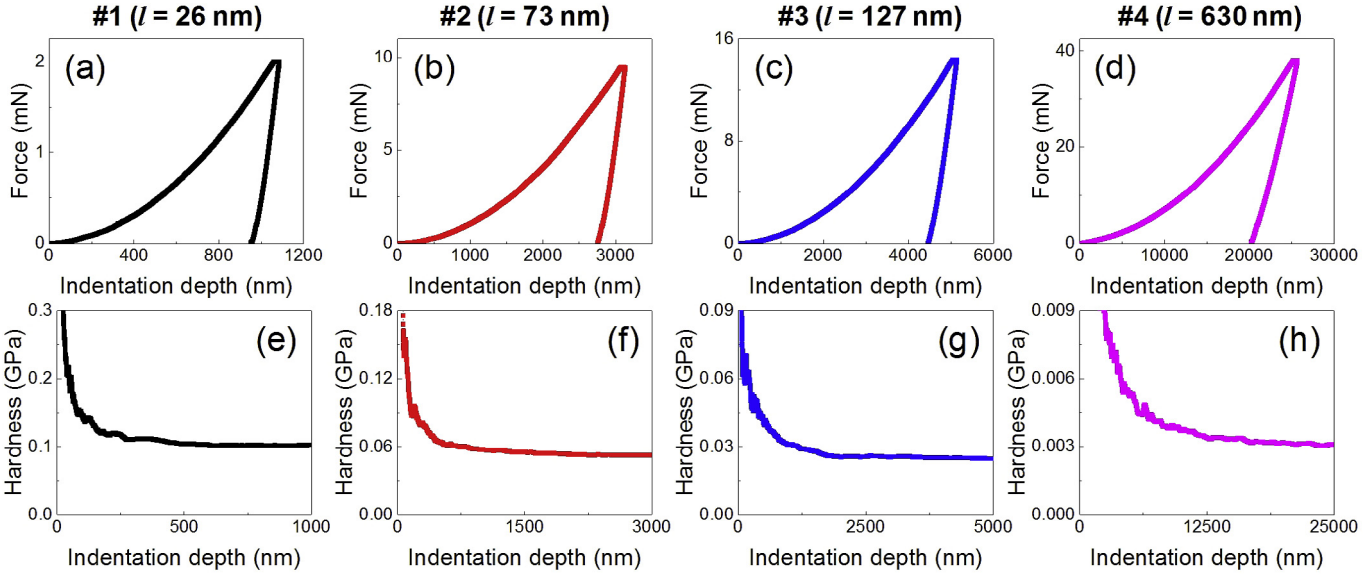

Fig. 2. (a)~(d) Typical nanoindentation force-depth curves and (e)~(h) typical relation of hardness and indentation depth for samples #1~#4.

convergent hardness at sufficient indentation depth is henceforth called the macroscopic hardness H_0; this value is 106.1 (±4.52) MPa for sample #1 (l = 26 nm), 55.8 (±1.62) MPa for sample #2 (l = 73 nm), 26.5 (±1.34) MPa for sample #3 (l = 127 nm), and 3.0 (±0.11) MPa for sample #4 (l = 630 nm).

For comparison for ligament-size-dependent hardness with previous results and the Gibson-Ashby model, the compressive yield strength σ_{comp} of np-Au as a function of ligament size is presented in Fig. 3. Our experimental results are evaluated by $\sigma_{comp} = H_0$ for four np-Au samples. It is important to note that recent results show plastic constrain factor Ψ for np-Au ranges from 2.65 to 3 similar to solid metals [19,22,32,33] rather than Ψ of 1 which is widely-used value for cellular materials with very low relative density [20,21]. We assume Ψ of 1 in this section to show trend for ligament-size-dependent hardness, however, in following sections, Ψ is not assumed to be 1 for modeling and analyzing experimental data. The green line is a scaling equation from Hodge et al.'s work [21] where Ψ of 1 is used, blue line is that from Briot et al.'s work [22] where Ψ of 2.65 (the measured value) is used. The red line indicates compressive strength of np-Au evaluated by the Gibson-Ashby model when ligament has strength of bulk annealed gold and np-Au has relative density ρ of 35%, which is the average relative density of samples #1~#4. The strength of bulk annealed gold was evaluated from a Vickers hardness value of 188 MPa [34] for bulk annealed gold by using $\Psi = 3$, the conventional assumption for solid metals; i.e., the red line was evaluated by $\sigma_{comp} = 0.3\frac{H}{3}\rho^{3/2}$. The compressive yield strength in Fig. 3, which is equal to macroscopic hardness for experimental results, shows strong ligament-size dependency for samples #1 (l = 26 nm) through #3 (l = 127 nm), consistent with previous work, and that for sample #4 (l = 630 nm) is close to the red line, implying that the strength of the ligament in sample #4 (l = 630 nm) is in the range of the strength of bulk annealed gold. We measured thickness of necks at the center of connections in ligaments that is possibly thinnest part in ligaments as 'ligament size'. Our ligament size could be expressed smaller comparing with previous works [21,22], which can explain that our experiments converge to bulk value earlier with increasing ligament size.

Fig. 4 shows typical relations between normalized hardness (ratio of hardness H to macroscopic hardness H_0) and normalized

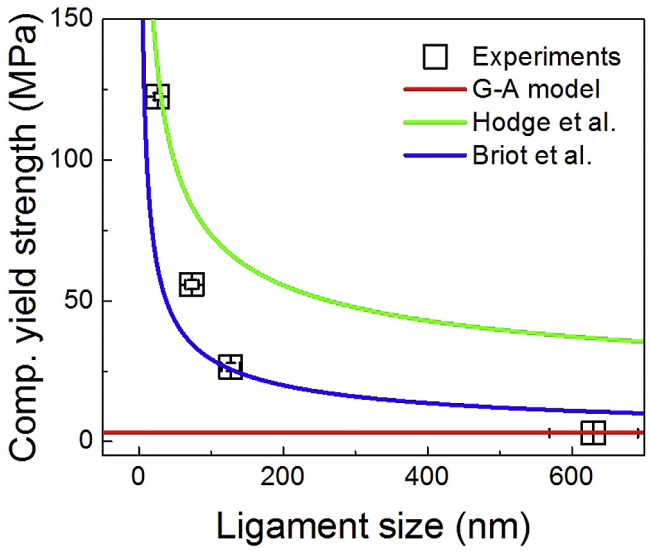

Fig. 3. Compressive yield strengths depending on ligament size in our experiments and previous reports. Some compressive yield strengths are converted from nano-indentation hardness. Red solid line indicates the Gibson-Ashby model ($\sigma^* = 0.3 \cdot 188/3 \cdot \left(\frac{\rho^*}{\rho_s}\right)^{\frac{3}{2}}$) [20], green line indicates equation suggested by Hodge et al. [21]. ($\sigma^* = 0.3\left[200 + 9821L^{-\frac{1}{2}}\right]\left(\frac{\rho^*}{\rho_s}\right)^{\frac{3}{2}}$), and blue line indicates equation suggested by Briot et al. ($\sigma^* = 1.939 \cdot 0.0328 \cdot l^{-0.551}\left(\frac{\rho^*}{\rho_s}\right)^{2.618}$) [22]. (For interpretation of the references to colour in this figure legend, the reader is referred to the web version of this article.)

indentation depth (ratio of indentation depth h to cell size D ($= 3l$)). This shows that trends of ISE for np-Au samples #1 ($l = 26$ nm), #2 ($l = 73$ nm) and #3 ($l = 126$ nm) are almost identical, while the ISE for sample #4 ($l = 630$ nm) is enhanced above the other three. These results mean that (1) an ISE, increase in hardness with decreasing indentation depth, is seen for four np-Au samples since it should be constant at 1 for the entire indentation depth in the case of no ISE, and (2) there is a ligament-size-dependent transition

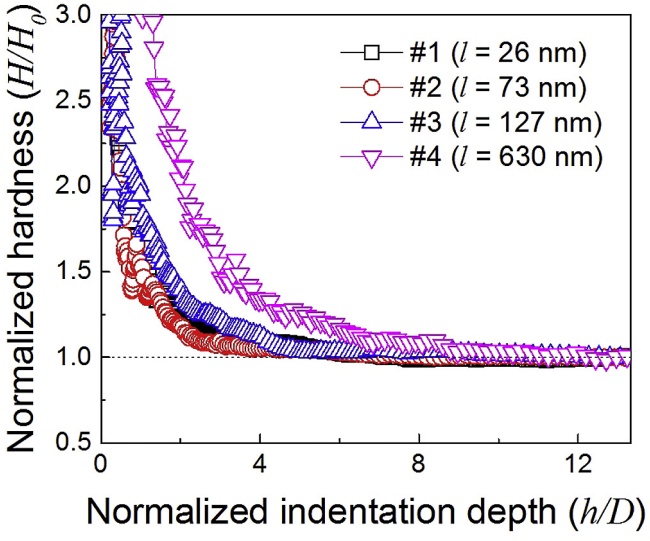

Fig. 4. Typical relations of normalized hardness and normalized indentation depth for samples #1~#4.

in ISE in np-Au because if there were not the ISE curves should overlap for all np-Au samples.

3.2. Nanomechanics modeling for nanoindentation on np-Au

To investigate the ligament-size-dependent ISE in np-Au, we develop a nanomechanics model for nanoindentation of np-Au with a sharp indenter such as Berkovich indenter. The sharp indenter is assumed to be composed of infinite thin disk-shape flat punches (Fig. 5). As loading in nanoindentation progresses as far as indentation depth δh, the perimeter area of $2\pi(r + \delta r)\delta h$ newly penetrates into np-Au mainly by shear force which induces initial plastic collapse of np-Au, and material volume in contact with the flat bottom penetrates by δh in the loading direction, and the bottom area is πr^2 that is the summation of segment $\pi(r + \delta r)^2 - \pi r^2$ from 0 to r with respect to r:

$$\sum_{n=0}^{r}\left[\pi(n+\delta r)^2 - \pi n^2\right] = \sum_{n=0}^{r}[\pi \cdot 2n\delta r] = \pi\int_0^r 2rdr = \pi r^2. \quad (1)$$

We simply assume that the unit length scale for plastic collapse of np-Au along the loading direction is one cell size D, which is the sum of one ligament and one pore, briefly assumed to be three times the ligament size $3l$. The relation between D and s, i.e. the spacing of individual steps by the nanoindent, is described as

$$\tan\theta = \frac{h}{r} = \frac{\delta h}{\delta r} = \frac{D}{s}, \quad s = \frac{Dr}{h}, \quad (2)$$

where θ is a contact angle between plane surface of sample and surface of indenter tip (19.7° for a Berkovich indenter) and r and h are contact radius and indentation depth, respectively, as shown in Fig. 5. The change in work introduced by nanoindentation, dW [28], when indentation depth increases by δh is given by

$$dW = \left(w_{\text{comp}} + w_{\text{shear}}\right)\frac{dr}{s}. \quad (3)$$

Here w_{comp} and w_{shear} are the work introduced by shear and compressive forces, respectively, described by

$$w_{\text{comp}} = \sigma \cdot \pi r^2 \cdot D, \quad (4a)$$

$$w_{\text{shear}} = \tau \cdot 2\pi r \cdot D \cdot kD, \quad (4b)$$

where σ and τ are the compressive and shear strength of np-Au, respectively, and k is a proportional constant that means the number of cells along the loading direction deformed by shear force at the perimeter $2\pi r \cdot D$ when indentation depth increases as much

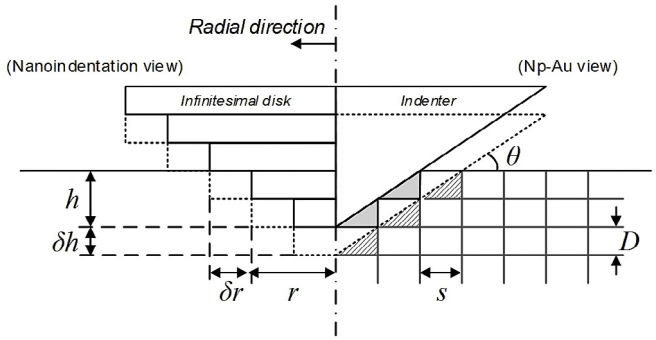

Fig. 5. Schematic on nanomechanics model for nanoindentation on np-Au.

as D [35,36]. σ and τ in Eqs. (4a) and (4b) are compressive and shear strength of bulk np-Au taking into consideration the inherent heterogeneity of np-Au, not for simplified nanoporous structure in simple stress modes [36]. The indentation force P can be described as

$$P = \frac{dW}{dh} = \sigma \cdot \pi r^2 + \tau \cdot 2\pi r \cdot kD. \quad (5)$$

Relation between hardness H and compressive strength σ can be described with plastic constraint factor Ψ as $H = \Psi\sigma$. By this relation, σ in Eq. (5) can be replaced by $(1/\Psi)H_0$ since σ is independent of indentation depth. Dividing both sides of Eq. (5) with the first term of the right side, $\sigma \cdot \pi r^2$ yields

$$\frac{H}{H_0} = \frac{1}{\Psi}\left(1 + \frac{K}{h/D}\right), \quad (6)$$

where

$$K = 2\tan\theta \cdot \frac{\tau}{\sigma} \cdot k. \quad (7)$$

Eq. (6) is the ISE model for np-Au, where H is the hardness, H_0 is the macroscopic hardness which is convergent with the hardness value at sufficient indentation depth, Ψ is the plastic constraint factor of np-Au, K is the characteristic length for the ISE for np-Au, and h/D is the indentation depth normalized by cell size. Eq. (6) is an inverse function of indentation depth, while the Nix-Gao model for solid materials is $\frac{H}{H_0} = \sqrt{1 + \frac{h^*}{h}}$, where h^* is the ISE characteristic length for solid materials [24]. At the early stage of research about mechanical behavior of np-Au, plastic constraint factor Ψ was assumed to be 1 as cellular materials with very low relative density with no comparison with tension and compression results of np-Au [20,21]. Recent studies revealed that plastic constraint factor for np-Au ranges from 2.65 to 3 similar to solid metals through comparison with tension and compression tests [19,22,32,33]. It is important to note that the characteristic length for the ISE for np-Au, K in Eq. (6) is independent of value of Ψ and only macroscopic hardness H_0 depends on value of Ψ. It is important to note that we assumed nanoporous structure is self-similar in this model. Kertis et al. [37] showed the self-similar aspect of np-Au with SEM images of ligament sizes from ~10^1 nm to ~10^3 nm by dealloying and post heat-treatments. Hu et al. [38] showed self-similarity of ligament connectivity in coarsened np-Au by using genus parameter. Chen-Wiegart et al. [39] measured three-dimensional structures of np-Au samples by three-dimensional tomographic reconstruction and segmentation. Based on these measurements, they could quantitatively propose that distributions of surface orientation and scaled surface curvature were not isotropic and consistent with coarsening time. Liu et al. [40] showed trends of mechanical self-similarity of np-Au in terms of network connectivity. They explained connectivity of each ligament by introducing an effective relative density, defined as a ratio of real and theoretical elastic moduli from compressive testing and theoretical Gibson-Ashby model. According to their results, the network connectivity of np-Au samples was gradually decreasing and showed a small increase above 100 nm of ligament size. Ziehmer et al. [41] concluded that coarsened np-Au might be self-similar. Jeon et al. [42] conducted 3D reconstruction of thermally-coarsened np-Au, and analyzed evolution of nanoporous structure during thermal coarsening. They found that np-Au coarsens in self-similar way in terms of distribution of ligament size, surface-to-volume ratio, and scaled connectivity density. Geometrically self-similarity of np-Au is still under debate. In this study, we assume self-similarity of np-Au is consistent during post heat-treatment to simplify the theoretical approach, leaving consideration of this issue to future studies.

Fig. 6(a)–(d) show that Eq. (6) successfully describes the typical relation of hardness vs indentation depth for samples #1-#4 as shown in Fig. 2(e) and (f). Fig. 6(e) shows the relation between normalized hardness and normalized indentation depth for samples #1-#4; here the curves were obtained by fitting Eq. (6) to more than 12 reproducible nanoindentation results for each sample. The characteristic constant K in Eq. (6) is 0.52 (±0.15) for sample #1 (l = 26 nm), 0.54 (±0.20) for sample #2 (l = 73 nm), 0.52 (±0.30) for sample #3 (l = 126 nm), and 1.86 (±0.47) for sample #4 (l = 630 nm), respectively. This result indicates that the trends of ISE for np-Au samples #1-#3 are almost identical and ISE for sample #4 is enhanced over the other three presumed in Fig. 4. Nanoindentations are basically assumed to have initial contact on the flat surface of solids. However, for np-Au, curved surfaces of ligaments and pores act as surface roughness, and this can affect hardness, especially at shallow indentation depths as reported in previous studies [28]. Fig. 6(f) shows a cross-sectional schematic illustration of nanoindentation on np-Au for possible cases of initial contact. The tip of a sharp indenter can make initial contact on top surface of ligament, indicated as 'top'. Also, it can be placed between two ligaments, and penetrate through pore, making initial contact between inclined plane of the sharp indenter and ligaments, indicated as 'bottom'. Since the line fitted with the proposed model between normalized hardness and normalized indentation depth in Fig. 6(e) was averaged for more than 12 reproducible nanoindentation results, the initial contact position for this case is indicated as 'average'. For the two extreme cases, the difference in indentation depth and the 'average' position is simply assumed to be $\pm 0.5h_0$. h_0 is easily evaluated with θ for a contact angle between sample surface and Berkovich indenter of 19.7° and measured ligament sizes for samples #1~#4, as required for modifying area functions. Expected deviations of normalized hardness with normalized indentation depth taking into account surface roughness effect of np-Au, are presented in Fig. 6(e) as dotted lines for each sample. The upper and lower dotted lines correspond to the cases of initial contact at 'top' and 'bottom' respectively, as described in Fig. 6(f). These boundaries are also presented as the possible range in k values in Fig. 9(b), which is discussed in section 3.4. Some amount of tip bluntness for sharp indenter is inevitable [26]. If the height difference between the ideally-sharp tip and the blunt tip, Δh_b is taken into account, height difference for the cases 'top' and 'bottom' initial contact, h_0 in Fig. 6(f) becomes h_0- Δh_b, which results in narrower gap between upper and lower boundaries in Fig. 6(e) and smaller scale bars of y-axis in Fig. 9(b). Blunt tip in sharp indenter can alleviate surface roughness effect in np-Au.

3.3. Compressive and shear strength

One parameter in Eq. (7) is the ratio of shear to compressive strengths, τ/σ, of np-Au. We performed uniaxial compression and pure shear tests for np-Au samples to obtain this ratio. Fig. 7(a) and (b) show typical compressive stress-strain curves. The compressive stress-strain curves for np-Au samples show three stages: linear elastic, plastic collapse, and densification which is typical compressive stress-strain behavior of porous materials [20]. We took the compressive strength σ in Eqs. (4a) and (7) as compressive yield strength determined by 0.2% offset method. The compressive yield strength measured in compression tests is 122.6 (±1.16) MPa for sample #1 (l = 26 nm), 41.5 (±4.30) MPa for sample #2 (l = 73 nm), 22.9 (±0.96) MPa for sample #3 (l = 126 nm), and 5.3 (±0.05) MPa for sample #4 (l = 630 nm). Fig. 7(c) shows the relation

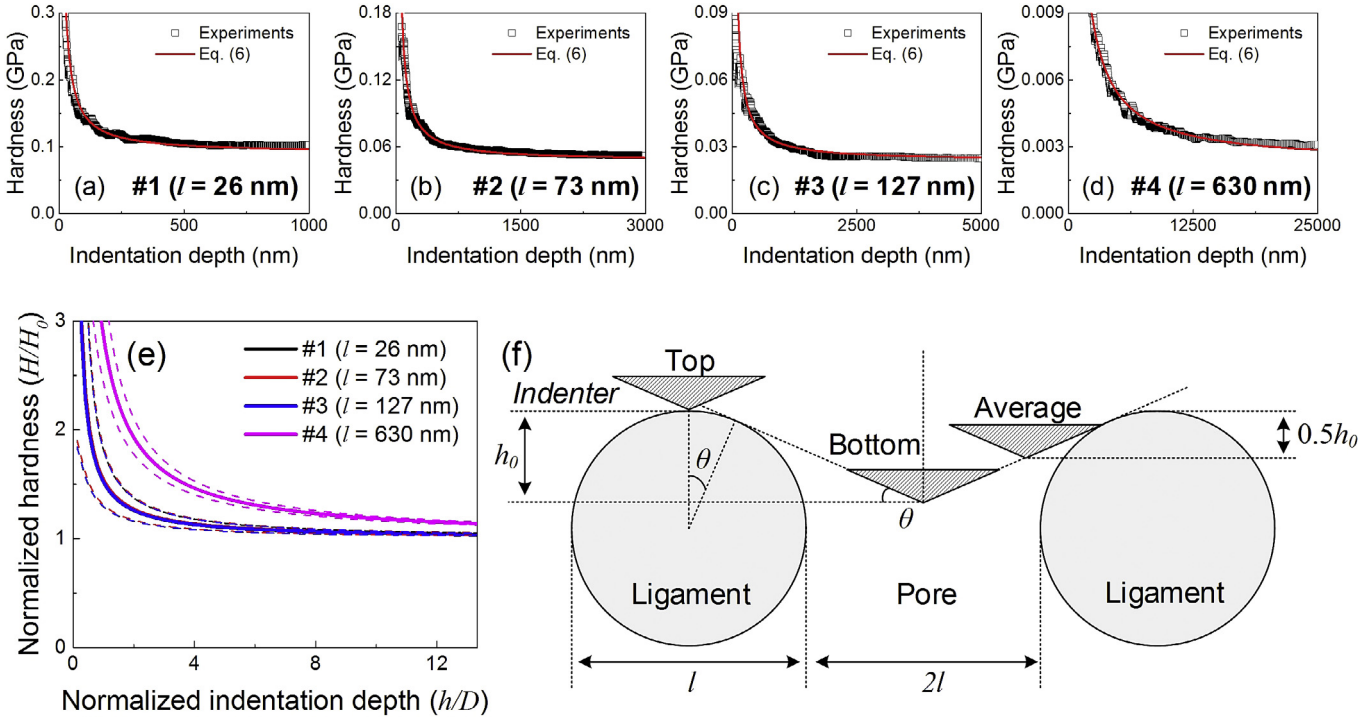

Fig. 6. (a)~(d) Experimental hardness as a function of indentation depth and Eq. (6) fitted to experiments for samples #1~#4; (e) average Eq. (6) obtained for each sample, upper and lower dotted lines correspond to the cases of initial contact at 'top' and 'bottom' respectively, as described in (f), indicating boundaries of possible normalized hardness caused by surface roughness effect in np-Au. (f) Schematic illustration of possible cases of initial contact between the tip of a sharp indenter and the surface of np-Au sample.

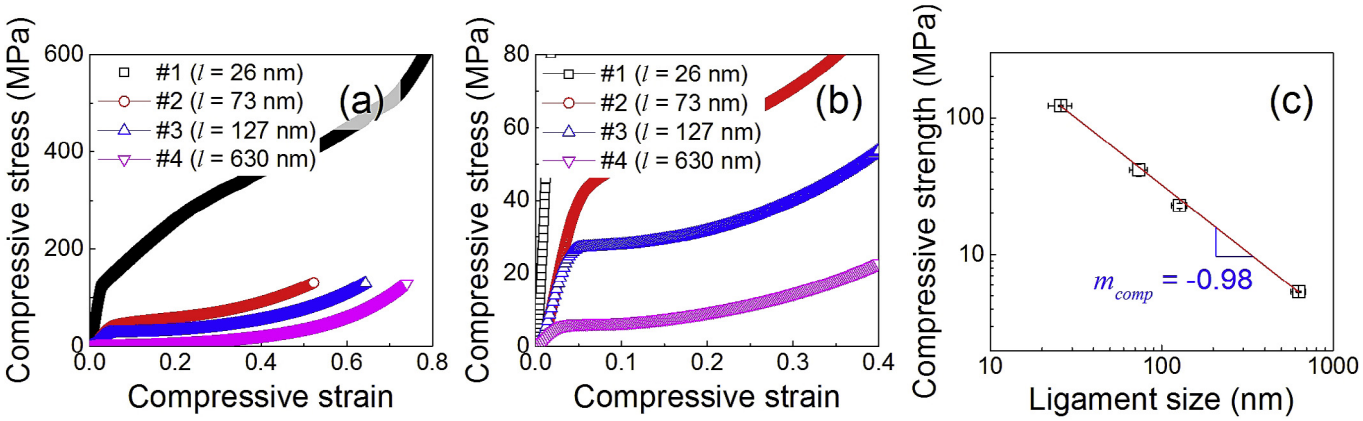

Fig. 7. (a) Compressive stress-strain curves for sample #1~#4; (b) enlarged compressive stress-strain curves; (c) relation of compressive strength and ligament size in log-log scale.

between compressive strength and ligament size in log-log scale: we see a linear relation with slope of 0.98, that is the size effect exponent, m_{comp} in $\sigma = l^{-m_{comp}}$.

Fig. 8(a) and (b) show typical pure shear stress-strain curves for np-Au samples. Samples #1~#3 show almost linear elastic deformation followed by catastrophic fracture. On the other hand, sample #4 (l = 630 nm) shows a linear elastic region, followed by continuous strain-hardening and strain-softening with increasing shear strain. Until a shear strain of 18%, sample #4 is not separated, while partial cracks are introduced. We took the shear strength τ in Eqs. (4a) and (7) as shear yield strength. The shear yield strength is 52.0 (±10.56) MPa for sample #1 (l = 26 nm), 7.6 (±1.36) MPa for sample #2 (l = 73 nm), and 1.5 (±0.34) MPa for sample #3 (l = 126 nm), respectively. The shear yield strength of sample #4 (l = 630 nm) determined by the 0.2% offset method is 0.3 (±0.06) MPa. The shear yield strength shows a strong ligament-size effect, m_{shear} is 1.60 in $\sigma = l^{-m_{shear}}$., as seen in Fig. 8(c). For samples #1~#3, the shear strength increases with decreasing ligament size by the size effect, the strength of ligament increases as ligament size decreases. However, these samples show catastrophic failure since increase in stress due to decrease in cross-sectional area of ligaments becomes greater than load-carrying ability of the ligaments due to strain-hardening. The shear stress-strain curve for sample #4 (l = 630 nm) indicates that strain-hardening is dominant in pure shear and shows transition in shear deformation mechanism from brittle to ductile between ligament size 126 nm (sample #3) and 630 nm (sample #4). Similar to our finding for ligament-size-dependent brittle to ductile transition in shear testing, Li and Sieradzki reported transition of ductile and brittle fracture of np-Au depending on ligament size in flexural testing [17].

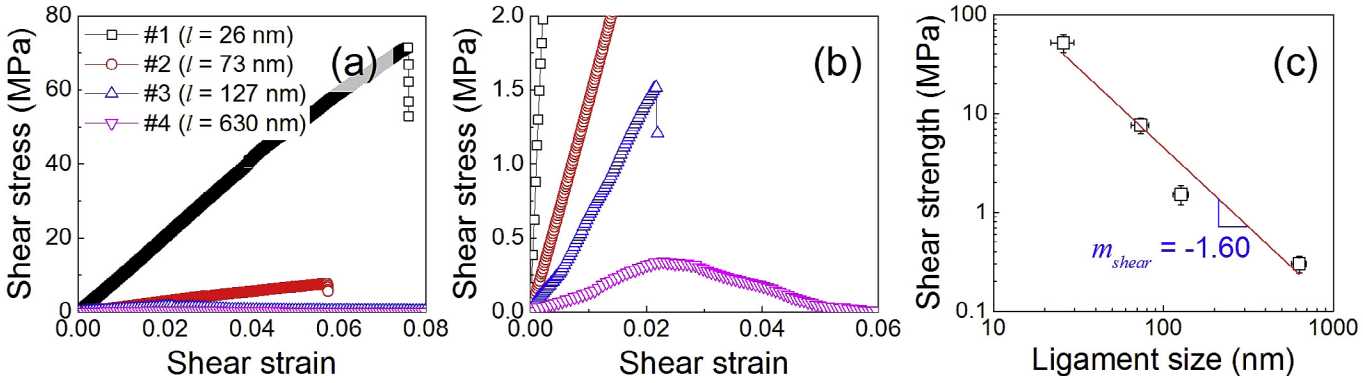

Fig. 8. (a) Shear stress-strain curves for sample #1~#4; (b) enlarged compressive stress-strain curves; (c) relation of shear strength and ligament size in log-log scale.

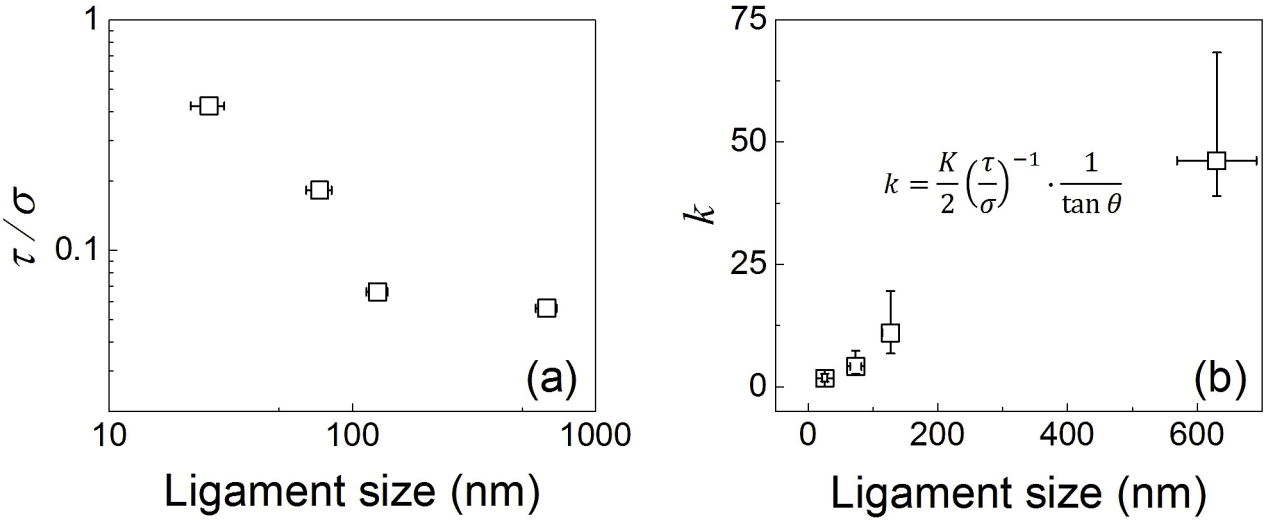

Fig. 9. (a) Ratio of shear strength to compressive strength and (b) k in Eqs. (4) and (7) as a function of ligament size. Error bars in k values correspond to the cases of initial contact at 'top' and 'bottom' respectively, as described in Fig. 6(f).

Fig. 9(a) shows the ratio of shear strength to compressive strength, τ/σ, as a function of ligament size. The ratio τ/σ is less than unity for all samples, i.e. shear strength is lower than compressive strength. Np-Au contains many dangling ligaments. If these ligaments are close enough to make contact during elastic deformation in compression, they support additional external compressive loading, leading to enhanced compressive strength. However, in shear testing, many of the separated neighboring ligaments become more distant since ligaments are stretched in shear mode and do not play the role of strengtheners. This difference could be attributed to the fact that the ratio τ/σ is less than unity. Balk et al. [43] reported a compressive strength of 15.5 MPa and a tensile strength of 11.5 MPa for polycrystalline np-Au with ligament size about 30 nm, yielding a ratio of tensile strength to compressive strength 0.74. In tensile loading, many separated neighboring ligaments are further separated and again have no strengthening role, and separation of grain boundaries can weaken tensile strength [16]. The ratio of tensile to compressive strength could be less than unity for the same reason. Meanwhile, it has been reported that a compressive strength of 22.5 MPa and a tensile strength of 25.3 MPa for single-crystalline np-Au with ligament size of 55.9 nm, yielding a ratio of tensile strength to compressive strength of 1.12 [44].

Fig. 9(b) shows k values depending on ligament size. The characteristic constant K was measured in section 3.2 and k values were obtained by substituting τ/σ in Eq. (7). Fig. 9(a) and (b) provide insight into origin of ISE in np-Au. For samples #1~#3, the ratio of shear strength to compressive strength, τ/σ, decreases and k increases with ligament size increases, and multiplication of them yields almost identical ISE characteristic constant K in Eq. (7). While sample #4 (l = 630 nm) has a similar (or slightly lower) ratio of shear strength to compressive strength τ/σ to sample #3 (l = 127 nm), it has much higher k value than samples #1~#3. Multiplication of τ/σ and k yields a much higher ISE characteristic constant K, leading to enhanced ISE over samples #1~#3 with smaller ligament size.

3.4. Origin of ligament-size-dependent ISE in np-Au

The size effect – increase in strength with decreasing ligament size – is clearly seen in both compression and shear strength in Figs. 7(c) and 8(c). Fig. 9(a) shows the dependency of the ratio of shear to compressive strength on ligament size: as ligament size increase, an overall decrease in the ratio and slightly lower ratio for sample #4 (l = 630 nm) than sample #3 (l = 127 nm). This trend comes from difference in the size effect exponents m, i.e. the slope of strength vs ligament size curve in log-log scale in Figs. 7(c) and 8(c). The size effect exponent for compressive strength, m_{comp}, is

0.98 (Fig. 7(c)) and that for shear strength, m_{shear}, is 1.60 (Fig. 8(c)). The size effect exponent for shear strength is 39% greater than that for compressive strength, which is caused by difference in deformation mode for shearing and compression.

Yield strength, showing power-law-type dependence on characteristic length of nano-structured materials, has been reported by numerous studies. Briot and Balk [22] calculated equivalent yield strength converted from nanoindentation hardness reported by Hodge et al. [21] by using a plastic constraint factor Ψ of 2.65, and obtained the power law exponent of −0.551 describing ligament-size-dependent yield strength. McCue et al. [33] analyzed the power law exponents calculated from experimental data obtained by 6 different mechanical tests reported by 17 previous research articles. Upper and lower boundaries for the power law exponents are −0.97 and −0.73, respectively. Obtained m_{comp} of −0.98 for compressive yield strength in this study is in good agreement with this trend. Li and Sieradzki [17] have reported ligament size dependent change in fracture stress with power law exponent of −0.2 from three-point bending tests. Badwe et al. [45] recently reported the power law exponent of −0.23 for tensile fracture stress for brittle fracture region corresponding to ligament size smaller than about 220 nm. Mameka et al. [46] recently found that phenomena that strength and hardness of np-Au increase as ligament size decreases is universal, but the power law exponents that had reported are quite diverse depending on materials and mechanical tests.

Greer et al. [47] measured compressive flow stress at 10% strain for Au micropillars with diameters ranging from 300 nm to 7450 nm. They found that the relation between flow stress and micropillar diameter can be described with two power-law exponents in transition at critical pillar diameter of about 1000 nm. Brinckmann et al. [48] showed that size-dependent compressive strength of Au nanopillars is described with the power law exponent of −0.97. The Hall-Petch relationship describing dependence of yield strength on grain size for nanocrystalline metals shows the power law exponent of −0.5 [49]. Deformation mechanism in np-Au might be similar to that of Au nanopillars in terms that mobile dislocations can escape at free surface due to external size of sub-micron scale, whereas dislocations can pile up at grain boundaries in nanocrystalline metals [50]. While entire volumes of nano- and micro-pillars are in uni-axial stress and strain conditions, ligaments in np-Au have surface curvature and irregular distribution in size and orientation introducing complex stress and strain in the ligaments, hence power-law exponents could be different from Au nano- and micro-pillars.

The size effect of materials at sub-micron scale is attributed to dislocation starvation or depletion of dislocation sources, since dislocations tend to escape at free surfaces and dislocations are exhausted due to small external size rather than multiplying as in bulk metals. In shear testing of np-Au, plastic deformation is likely localized at necks of ligaments, possibly the thinnest part in ligaments. Dislocation starvation model that take into account size effect in Au nanopillar compression could be applied to shear strength of np-Au since the dislocations on ligament surface can travel through ligament and escape at the opposite free surface of ligament. Ngo et al. [51] suggested that initial yielding in compression of np-Au occurs at very early stage of loading due to surface-induced prestress and anomalously high elastic compliance through MD simulations. They also found that typical dislocation-based mechanism contributes to the strain hardening of np-Au during compressive deformation while dislocation-starvation model is not applied to np-Au under compression. Unlike nano- and micro-pillars with uniform geometry, curvature, size, and orientation of ligaments in np-Au are naturally irregular. Structural irregularity might elucidate unique deformation behavior that stress can be concentrated at the thinnest parts [52], possibly necks of ligaments and existence or density of initial dislocation in volumes of necks is more critical in yielding rather than overall initial dislocation density. We calculated total initial dislocation length in disc-shaped volume with diameter of average ligament size and thickness of one diameter. Thickness of disc is briefly assumed to be one diameter of ligament where stress is highly concentrated. When initial dislocation density is assumed as 10^9 m^{-2} [53], total dislocation length in the neck volume is 1.38 × 10^{-5} nm for ligament size $l = 26$ nm (sample #1) and that is 0.2 nm for $l = 630$ nm (sample #4). This means that rare initial dislocations are statistically included in the neck volumes that is critical in yielding. These fundamental differences in yielding mechanism under shear and compressive deformation could result in disparity of the power law exponents. The difference in the size effect exponent m in shear and compressive strengths yields a trend of τ/σ as a function of ligament size, as shown in Fig. 9(a), and this is attributed to origin of ligament-size-dependent ISE in np-Au.

Fig. 9(b) shows that k, the proportional constant in Eq. (7), is proportional to ligament size. In the suggested nanomechanics model, k means the number of deformed cells along the loading direction by shear force at the perimeter $2\pi r \cdot D$ when indentation depth increases as much as D. In realistic nanoindentation on np-Au, it is difficult to define k. Instead, one can realize intuitively that k is associated with the depth at which shear stress, introduced at the contact boundary between the np-Au surface and nanoindenter, is applied. In terms of normalized indentation depth, the strength of ligaments decreases with ligament size; i.e. in identical configurations of ligaments and pores for samples #1-#4, only the ligament strength is different. The increase in k with increasing ligament size indicates that shear stress introduced at contact boundary is applied farther as ligament strength decreases in terms of normalized indentation depth. The ISE in np-Au is thus attributed to a combination of ligament-size-dependent τ/σ and k shown in Fig. 9(a) and (b).

4. Conclusion

We found that the ISE for np-Au depends on ligament size. Np-Au of ligament sizes 26, 73, and 126 nm showed almost identical ISE, while np-Au of ligament size 630 nm showed relatively enhanced ISE. To investigate this ligament-size-dependent ISE in np-Au, we established a nanomechanics model for nanoindentation on np-Au. We assumed that the total work of nanoindentation consists of two dissipated works: the work introduced by shear forces to slide ligaments at the perimeter around the nanoindenter, and the work introduced by compressive force to collapse ligaments beneath the nanoindenter. From this derived force and Tabor's relation, a hardness normalized by macroscopic hardness was described as a function of indentation depth normalized by unit cell size, simply twice ligament size. On the basis of this theoretical approach, a ligament-size-dependent ISE model was developed as an inverse function and applied to our experimental results. The ISE in np-Au resulted from the difference in size-effect exponents in compression and shear loading depending on ligament sizes, where the size effect in shear strength depended more on ligament size than that in compressive strength. This phenomenon was explained by dislocation movements toward thinner connections in ligaments and thicker junctions in ligaments, resulting in a tendency to greater strain-hardening by dislocation pile-up. To verify the model and the explanation of ISE, we performed shear and compressive testing with millimeter-scale rectangular np-Au samples. The ratio of shear to compressive strength depends on ligament size. The combination of a linear increase in k and a convergent decrease in τ/σ caused by different

size-effect exponents in shear and compressive strength with increasing ligament size explains the ISE transition between ligament sizes of 126 and 630 nm.

Acknowledgments

This work was supported by the National Research Foundation of Korea (NRF) grant funded by the Ministry of Science, ICT & Future Planning (MSIP) (NO. NRF-2015R1A5A1037627), by the KIST-UNIST partnership program (1.160097.01/2.160482.01), and by the National Research Foundation of Korea (NRF) grant funded by the Korea goverment (MSIP) (NO. NRF-2017R1C1B2009329).

References

[1] J. Erlebacher, M.J. Aziz, A. Karma, N. Dimitrov, K. Sieradzki, Evolution of nanoporosity in dealloying, Nature 410 (2001) 450–453.
[2] D. Kramer, R.N. Viswanath, J. Weissmuller, Surface-stress induced macroscopic bending of nanoporous gold cantilevers, Nano Lett. 4 (2004) 793–796.
[3] Y. Ding, Y.J. Kim, J. Erlebacher, Nanoporous gold leaf: “Ancient technology”/advanced material, Adv. Mater. 16 (2004) 1897.
[4] F. Jia, C. Yu, Z. Ai, L. Zhang, Fabrication of nanoporous gold film electrodes with ultrahigh surface area and electrochemical activity, Chem. Mater. 19 (2007) 3648–3653.
[5] K. Hu, D. Lan, X. Li, S. Zhang, Electrochemical DNA biosensor based on nanoporous gold electrode and multifunctional encoded DNA-Au bio bar codes, Anal. Chem. 80 (2008) 9124–9130.
[6] J. Biener, A. Wittstock, L.A. Zepeda-Ruiz, M.M. Biener, V. Zielasek, D. Kramer, R.N. Viswanath, J. Weissmueller, M. Baeumer, A.V. Hamza, Surface-chemistry-driven actuation in nanoporous gold, Nat. Mater. 8 (2009) 47–51.
[7] A. Wittstock, V. Zielasek, J. Biener, C.M. Friend, M. Baeumer, Nanoporous gold catalysts for selective gas-phase oxidative coupling of methanol at low temperature, Science 327 (2010) 319–322.
[8] E. Detsi, Z.G. Chen, W.P. Vellinga, P.R. Onck, J.T.M. De Hosson, Reversible strain by physisorption in nanoporous gold, Appl. Phys. Lett. 99 (2011) 083104.
[9] M.M. Biener, J. Biener, A. Wichmann, A. Wittstock, T.F. Baumann, M. Baeumer, A.V. Hamza, ALD functionalized nanoporous gold: thermal stability, mechanical properties, and catalytic activity, Nano Lett. 11 (2011) 3085–3090.
[10] E. Detsi, Z.G. Chen, W.P. Vellinga, P.R. Onck, J.T.M.D. Hosson, Actuating and sensing properties of nanoporous gold, J. Nanosci. Nanotechnol. 12 (2012) 4951–4955.
[11] T. Fujita, P. Guan, K. McKenna, X. Lang, A. Hirata, L. Zhang, T. Tokunaga, S. Arai, Y. Yamamoto, N. Tanaka, Y. Ishikawa, N. Asao, Y. Yamamoto, J. Erlebacher, M. Chen, Atomic origins of the high catalytic activity of nanoporous gold, Nat. Mater. 11 (2012) 775–780.
[12] E. Detsi, S. Punzhin, J. Rao, P.R. Onck, J.T.M. De Hosson, Enhanced strain in functional nanoporous gold with a dual microscopic length scale structure, ACS Nano 6 (2012) 3734–3744.
[13] E. Detsi, P.R. Onck, J.T.M. De Hosson, Electrochromic artificial muscles based on nanoporous metal-polymer composites, Appl. Phys. Lett. 103 (2013) 193101.
[14] E. Detsi, P. Onck, J.T.M. De Hosson, Metallic muscles at work: high rate actuation in nanoporous gold/polyaniline composites, ACS Nano 7 (2013) 4299–4306.
[15] J. Biener, A.M. Hodge, A.V. Hamza, Microscopic failure behavior of nanoporous gold, Appl. Phys. Lett. 87 (2005) 121908.
[16] E.J. Gwak, J.Y. Kim, Weakened flexural strength of nanocrystalline nanoporous gold by grain refinement, Nano Lett. 16 (2016) 2497–2502.
[17] R. Li, K. Sieradzki, Ductile-brittle transition in random porous Au, Phys. Rev. Lett. 68 (1992) 1168–1171.
[18] J. Biener, A.M. Hodge, J.R. Hayes, C.A. Volkert, L.A. Zepeda-Ruiz, A.V. Hamza, F.F. Abraham, Size effects on the mechanical behavior of nanoporous Au, Nano Lett. 6 (2006) 2379–2382.
[19] C.A. Volkert, E.T. Lilleodden, D. Kramer, J. Weissmüller, Approaching the theoretical strength in nanoporous Au, Appl. Phys. Lett. 89 (2006) 061920.
[20] L.J. Gibson, M.F. Ashby, Cellular Solids: Structure and Properties, second ed., Cambridge University Press, Cambridge, 1997.
[21] A.M. Hodge, J. Biener, J.R. Hayes, P.M. Bythrow, C.A. Volkert, A.V. Hamza, Scaling equation for yield strength of nanoporous open-cell foams, Acta Mater. 55 (2007) 1343–1349.
[22] N.J. Briot, T.J. Balk, Developing scaling relations for the yield strength of nanoporous gold, Philos. Mag. 95 (2015) 2955–2973.
[23] S.S.R. Saane, K.R. Mangipudi, K.U. Loos, J.T.M. De Hosson, P.R. Onck, Multiscale modeling of charge-induced deformation of nanoporous gold structures, J. Mech. Phys. Solids 66 (2014) 1–15.
[24] W.D. Nix, H.J. Gao, Indentation size effects in crystalline materials: a law for strain gradient plasticity, J. Mech. Phys. Solids 46 (1998) 411–425.
[25] K. Durst, B. Backes, M. Goken, Indentation size effect in metallic materials: correcting for the size of the plastic zone, Scr. Mater. 52 (2005) 1093–1097.
[26] J.-Y. Kim, B.-W. Lee, D.T. Read, D. Kwon, Influence of tip bluntness on the size-dependent nanoindentation hardness, Scr. Mater. 52 (2005) 353–358.
[27] Y. Huang, F. Zhang, K.C. Hwang, W.D. Nix, G.M. Pharr, G. Feng, A model of size effects in nano-indentation, J. Mech. Phys. Solids 54 (2006) 1668–1686.
[28] J.-Y. Kim, S.-K. Kang, J.-J. Lee, J.-i. Jang, Y.-H. Lee, D. Kwon, Influence of surface-roughness on indentation size effect, Acta Mater. 55 (2007) 3555–3562.
[29] B.-W. Choi, D.-H. Seo, J.-i. Jang, A nanoindentation study on the micromechanical characteristics of API X100 pipeline steel, Metals Mater. Int. 15 (2009) 373–378.
[30] G.M. Pharr, E.G. Herbert, Y. Gao, The indentation size effect: a critical examination of experimental observations and mechanistic interpretations, in: D.R. Clarke, M. Ruhle, F. Zok (Eds.), Annu. Rev. Mater. Res. 40 (2010) 271–292.
[31] E.-J. Gwak, N.-R. Kang, U.B. Baek, H.M. Lee, S.H. Nahm, J.-Y. Kim, Microstructure evolution in nanoporous gold thin films made from sputter-deposited precursors, Scr. Mater. 69 (2013) 720–723.
[32] H.J. Jin, L. Kurmanaeva, J. Schmauch, H. Rosner, Y. Ivanisenko, J. Weissmuller, Deforming nanoporous metal: role of lattice coherency, Acta Mater. 57 (2009) 2665–2672.
[33] I. McCue, E. Benn, B. Gaskey, J. Erlebacher, Dealloying and dealloyed materials, Annu. Rev. Mater. Res. 46 (2016) 263–286.
[34] G.V. Samsonov, Mechanical properties of the elements, in: Handbook of the Physicochemical Properties of the Elements, IFI-Plenum, New York, USA, 1968.
[35] E.W. Andrews, G. Gioux, P. Onck, L.J. Gibson, Size effects in ductile cellular solids. Part II: experimental results, Int. J. Mech. Sci. 43 (2001) 701–713.
[36] P.R. Onck, E.W. Andrews, L.J. Gibson, Size effects in ductile cellular solids. Part I: modeling, Int. J. Mech. Sci. 43 (2001) 681–699.
[37] F. Kertis, J. Snyder, L. Govada, S. Khurshid, N. Chayen, J. Erlebacher, Structure/processing relationships in the fabrication of nanoporous gold, Jom-Us 62 (2010) 50–56.
[38] K. Hu, M. Ziehmer, K. Wang, E.T. Lilleodden, Nanoporous gold: 3D structural analyses of representative volumes and their implications on scaling relations of mechanical behaviour, Philos. Mag. 96 (2016) 3322–3335.
[39] Y.C.K. Chen-Wiegart, S. Wang, Y.S. Chu, W.J. Liu, I. McNulty, P.W. Voorhees, D.C. Dunand, Structural evolution of nanoporous gold during thermal coarsening, Acta Mater. 60 (2012) 4972–4981.
[40] L.-Z. Liu, X.-L. Ye, H.-J. Jin, Interpreting anomalous low-strength and low-stiffness of nanoporous gold: quantification of network connectivity, Acta Mater. 118 (2016) 77–87.
[41] M. Ziehmer, K. Hu, K. Wang, E.T. Lilleodden, A principle curvatures analysis of the isothermal evolution of nanoporous gold: quantifying the characteristic length-scales, Acta Mater. 120 (2016) 24–31.
[42] H. Jeon, N.R. Kang, E.J. Gwak, J.I. Jang, H.N. Han, J.Y. Hwang, S. Lee, J.Y. Kim, Self-similarity in the structure of coarsened nanoporous gold, Scr. Mater. 137 (2017) 46–49.
[43] T.J. Balk, C. Eberl, Y. Sun, K.J. Hemker, D.S. Gianola, Tensile and compressive microspecimen testing of bulk nanoporous gold, Jom-Us 61 (2009) 26–31.
[44] N.J. Briot, T. Kennerknecht, C. Eberl, T.J. Balk, Mechanical properties of bulk single crystalline nanoporous gold investigated by millimetre-scale tension and compression testing, Philos. Mag. 94 (2014) 847–866.
[45] N. Badwe, X. Chen, K. Sieradzki, Mechanical properties of nanoporous gold in tension, Acta Mater. 129 (2017) 251–258.
[46] N. Mameka, K. Wang, J. Markmann, E.T. Lilleodden, J. Weissmüller, Nanoporous gold—testing macro-scale samples to probe small-scale mechanical behavior, Mater. Res. Lett. 4 (2016) 27–36.
[47] J.R. Greer, W.C. Oliver, W.D. Nix, Size dependence of mechanical properties of gold at the micron scale in the absence of strain gradients, Acta Mater. 53 (2005) 1821–1830.
[48] S. Brinckmann, J.Y. Kim, J.R. Greer, Fundamental differences in mechanical behavior between two types of crystals at the nanoscale, Phys. Rev. Lett. 100 (2008).
[49] M.A. Meyers, A. Mishra, D.J. Benson, Mechanical properties of nanocrystalline materials, Prog. Mater. Sci. 51 (2006) 427–556.
[50] J.R. Greer, J.T.M. De Hosson, Plasticity in small-sized metallic systems: intrinsic versus extrinsic size effect, Prog. Mater. Sci. 56 (2011) 654–724.
[51] B.-N.D. Ngô, A. Stukowski, N. Mameka, J. Markmann, K. Albe, J. Weissmüller, Anomalous compliance and early yielding of nanoporous gold, Acta Mater. 93 (2015) 144–155.
[52] X.-Y. Sun, G.-K. Xu, X. Li, X.-Q. Feng, H. Gao, Mechanical properties and scaling laws of nanoporous gold, J. Appl. Phys. 113 (2013) 023505.
[53] D. Hull, D.J. Bacon, Introduction to Dislocations, third ed., Pergamon Press, Oxford Oxfordshire, New York, 1984.